# The Dynamics of Tibetan Singing Bowls

Octávio Inácio & Luís L. Henrique
Instituto Politécnico do Porto, Escola Superior de Música e Artes do Espectáculo, Musical Acoustics Laboratory, Rua da Alegria, 503, 4000-045 Porto, Portugal

José Antunes
Instituto Tecnológico e Nuclear, Applied Dynamics Laboratory ITN/ADL, Estrada Nacional 10, 2686-953 Sacavém Codex, Portugal

**Summary**

Tibetan bowls have been traditionally used for ceremonial and meditation purposes, but are also increasingly being used in contemporary music-making. They are handcrafted using alloys of several metals and produce different tones, depending on the alloy composition, their shape, size and weight. Most important is the sound-producing technique used – either impacting or rubbing, or both simultaneously – as well as the excitation location, the hardness and friction characteristics of the exciting stick (called *puja*). Recently, researchers became interested in the physical modelling of singing bowls, using waveguide synthesis techniques for performing numerical simulations. Their efforts aimed particularly at achieving real-time synthesis and, as a consequence, several aspects of the physics of these instruments do not appear to be clarified in the published numerical formulations and results. In the present paper, we extend to axi-symmetrical shells – subjected to impact and friction-induced excitations – our modal techniques of physical modelling, which were already used in previous papers concerning plucked and bowed strings as well as impacted and bowed bars. We start by an experimental modal identification of three different Tibetan bowls, and then develop a modelling approach for these systems. Extensive nonlinear numerical simulations were performed, for both impacted and rubbed bowls, which in particular highlight important aspects concerning the spatial patterns of the friction-induced bowl vibrations. Our results are in good agreement with preliminary qualitative experiments.

**PACS no. 43.75.Kk**

## 1. Introduction

Several friction-excited idiophones are familiar to western musical culture, such as bowed vibraphone and marimba bars, the nail violin, the musical saw, musical glasses and the glass harmonica, as well as some natural objects rubbed against each other, like sea shells, bones, stones or pine-cones. In an interesting tutorial paper, Akay [1] presents an overview of the acoustics phenomena related to friction, which is the main sound-generating mechanism for such systems. Some of these musical instruments have been experimentally studied, in particular by Rossing and co-workers, an account of which will be found in [2]. Nevertheless, the analysis of idiophones excited by friction is comparatively rare in the literature and mostly recent – see French [3], Rossing [4], Chapuis [5] and Essl & Cook [6]. Among these studies, only [3] and [6] aim at physical modelling, respectively of rubbed glasses and bowed bars. In our previous work – Inácio et al. [7-9] – we also investigated the stick-slip behaviour of bowed bars under different playing

This paper is an enlarged version of work presented at the 34th Spanish National Acoustics Congress and EEA Symposium (Tecniacústica 2003) and at the International Symposium on Musical Acoustics (ISMA 2004), Japan.

conditions, using a modal approach and a simplified friction model for the bow/bar interaction.

Recently, some researchers became interested in the physical modelling of singing bowls, using waveguide synthesis techniques for performing numerical simulations [10-12]. Their efforts aimed particularly at achieving real-time synthesis. Therefore, understandably, several aspects of the physics of these instruments do not appear to be clarified in the published formulations and results. For instance, to our best knowledge, an account of the radial and tangential vibratory motion components of the bowl shell – and their dynamical coupling – has been ignored in the published literature. Also, how these motion components relate to the travelling position of the *puja* contact point is not clear at the present time. Details of the contact/friction interaction models used in simulations have been seldom provided, and the significance of the various model parameters has not been asserted. On the other hand, experiments clearly show that beating phenomena arises even for near-perfectly symmetrical bowls, an important aspect which the published modelling techniques seem to miss (although beating from closely mistuned modes has been addressed – not without some difficulty [12] – but this is a quite different aspect). Therefore, it appears that several important aspects of the excitation mechanism in singing bowls still lack clarification.

In this paper, we report and extend our recent studies [13,14] by applying the modal physical modelling techniques to axi-symmetrical shells subjected to impact and/or friction-induced excitations. These techniques were already used in previous papers concerning plucked and bowed strings [15-18] as well as impacted [19] and bowed bars [7-9]. Our approach is based on a modal representation of the unconstrained system – here consisting on two orthogonal families of modes of similar (or near-similar) frequencies and shapes. The bowl modeshapes have radial and tangential motion components, which are prone to be excited by the normal and frictional contact forces between the bowl and the impact/sliding *puja*. At each time step, the generalized (modal) excitations are computed by projecting the normal and tangential interaction forces on the modal basis. Then, time-step integration of the modal differential equations is performed using an explicit algorithm. The physical motions at the contact location (and any other selected points) are obtained by modal superposition. This enables the computation of the motion-dependent interaction forces, and the integration proceeds. Details on the specificities of the contact and frictional models used in our simulations are given. A detailed experimental modal identification has been performed for three different Tibetan bowls. Then, we produce an extensive series of nonlinear numerical simulations, for both impacted and rubbed bowls, demonstrating the effectiveness of the proposed computational techniques and highlighting the main features of the physics of singing bowls. We discuss extensively the influence of the contact/friction and playing parameters – the normal contact force $F_N$ and of the tangential velocity $V_T$ of the exciter – on the produced sounds. Many aspects of the bowl responses displayed by our numerical simulations have been observed in preliminary qualitative experiments.

Our simulation results highlight the existence of several motion regimes, both steady and unsteady, with either permanent or intermittent bowl/*puja* contact. Furthermore, the unstable modes spin at the angular velocity of the *puja*. As a consequence, for the listener, singing bowls behave as rotating quadropoles. The sound will always be perceived as beating phenomena, even if using perfectly symmetrical bowls. From our computations, sounds and animations have been produced, which appear to agree with qualitative experiments. Some of the computed sounds are appended to this paper.

## 2. Tibetan singing bowls and their use

Singing bowls, also designated by Himalayan or Nepalese singing bowls [20] are traditionally made in

Tibet, Nepal, Bhutan, Mongolia, India, China and Japan. Although the name *qing* has been applied to lithophones since the Han Chinese Confucian rituals, more recently it also designates the bowls used in Buddhist temples [21]. In the Himalaya there is a very ancient tradition of metal manufacture, and bowls have been handcrafted using alloys of several metals – mainly copper and tin, but also other metals such as gold, silver, iron, lead, etc. – each one believed to possess particular spiritual powers. There are many distinct bowls, which produce different tones, depending on the alloy composition, their shape, size and weight. Most important is the sound producing technique used – either impacting or rubbing, or both simultaneously – as well as the excitation location, the hardness and friction characteristics of the exciting stick (called *puja*, frequently made of wood and eventually covered with a soft skin) – see [22].

The origin of these bowls isn't still well known, but they are known to have been used also as eating vessels for monks. The singing bowls dates from the Bon civilization, long before the Buddhism [23]. Tibetan bowls have been used essentially for ceremonial and meditation purposes. Nevertheless, these amazing instruments are increasingly being used in relaxation, meditation [23], music therapy [20, 24, 25] and contemporary music.

The musical use of Tibetan singing bowls in contemporary music is a consequence of a broad artistic movement. In fact, in the past decades the number of percussion instruments used in Western music has greatly increased with an "invasion" of many instruments from Africa, Eastern, South-America and other countries. Many Western composers have included such instruments in their music in an acculturation phenomenon.

The Tibetan bowls and other related instruments used in contemporary music are referred to, in scores, by several names: temple bells, campana di templo, japonese temple bell, Buddhist bell, cup bell, dobaci Buddha temple bell. Several examples of the use of these instruments can be found in contemporary music: Philippe Leroux, *Les Uns* (2001); John Cage/Lou Harrison, *Double Music* (1941) percussion quartet, a work with a remarkable Eastern influence; Olivier Messiaen, *Oiseaux Exotiques* (1955/6); John Kenneth Tavener, cantata *Total Eclipse* (1999) for vocal soloist, boys' choir, baroque instruments, brass, Tibetan bowls, and timpani; Tan Dun Opera *Marco Polo* (1995) with Tibetan bells and Tibetan singing bowls; Joyce Bee Tuan Koh, *Lè* (1997) for choir and Tibetan bowls.

Figure 1. Three singing bowls used in the experiments: Bowl 1 ($\phi$ = 180 mm); Bowl 2 ($\phi$ = 152 mm); Bowl 3 ($\phi$ = 140 mm).

Figure 2. Large singing bowl: Bowl 4 ($\phi$ = 262 mm), and two pujas used in the experiments.

## 3. Experimental modal identification

Figures 1 and 2 show the four bowls and two *pujas* used for the experimental work in this paper. In order to estimate the natural frequencies $\omega_n$, damping values $\varsigma_n$, modal masses $m_n$ and modeshapes $\varphi_n(\theta, z)$ to be used in our numerical simulations, a detailed experimental modal identification based on impact testing was performed for Bowls 1, 2 and 3. A mesh of 120 test locations was defined for each instrument (e.g., 24 points regularly spaced azimuthally, at 5 different heights). Impact excitation was performed on all of the points and

the radial responses were measured by two accelerometers attached to inner side of the bowl at two positions, located at the same horizontal plane (near the rim) with a relative angle of 55º between them, as can be seen in Figure 3(a). Modal identification was achieved by developing a simple MDOF algorithm in the frequency domain [26]. The modal parameters were optimized in order to minimize the error $\varepsilon(\omega_n, \varsigma_n, m_n, \varphi_n)$ between the measured transfer functions $H_{er}(\omega) = \ddot{Y}_r(\omega) \big/ F_e(\omega)$ and the fitted modal model $\hat{H}_{er}(\omega; \omega_n, \varsigma_n, m_n, \varphi_n)$, for all measurements ($P_e$ excitation and $P_r$ response locations), in a given frequency range $[\omega_{\min}, \omega_{\max}]$ encompassing $N$ modes. Hence:

$$\begin{aligned} &\varepsilon(\omega_n, \varsigma_n, m_n, \varphi_n) = \\ &= \sum_{e=1}^{P_e} \sum_{r=1}^{P_r} \int_{\omega_{\min}}^{\omega_{\max}} \left[ H_{er}(\omega) - \hat{H}_{er}(\omega; \omega_n, \varsigma_n, m_n, \varphi_n) \right] d\omega \end{aligned} \tag{1}$$

with:

$$\begin{aligned} &\hat{H}_{er}(\omega; \omega_n, \varsigma_n, m_n, \varphi_n) = \\ &= \sum_{n=n_1}^{n_1+N} -\omega^2 \frac{A_n^{er}}{\omega_n^2 - \omega^2 + 2i\omega\omega_n\varsigma_n} - \omega^2 C_1 + C_2 \end{aligned} \tag{2}$$

where the modal amplitude coefficients are given as $A_n^{er} = \varphi_n(\theta_e, z_e)\varphi_n(\theta_r, z_r)/m_n$ and the two last terms in (2) account for modes located out of the identified frequency-range. The values of the modal masses obviously depend on how modeshapes are normalized (we used $|\varphi(\theta, z)|_{\max} = 1$). Note that the identification is nonlinear in $\omega_n$ and $\varsigma_n$ but linear in $A_n^{er}$.

Results from the experiments on the three bowls show the existence of 5 to 7 prominent resonances with very low modal damping values up to frequencies about 4 ~ 6 kHz. For these well-defined experimental modes, the simple identification scheme used proved adequate. As an illustration, Figure 3(b) depicts the modulus of a frequency response function obtained from Bowl 2, relating the acceleration measured at point 1 (near the bowl rim) to the force applied at the same point.

The shapes of the identified bowl modes are mainly due to bending waves that propagate azimuthally, resulting in patterns similar to some modeshapes of bells [2]. Following Rossing, notation $(j,k)$ represents here the number of complete nodal meridians extending over the top of the bowl (half the number of nodes observed along a circumference), and the number of nodal circles, respectively.

Despite the high manufacturing quality of these handcrafted instruments, perfect axi-symmetry is nearly impossible to achieve. As will be explained in section 4, these slight geometric imperfections lead to the existence of two orthogonal modes (hereby called modal families A and B), with slightly different natural frequencies. Although this is not apparent in Figure 3(b), by zooming the analysis frequency-range, an apparently single resonance often reveals two closely spaced peaks.

Figure 4 shows the perspective and top views of the two orthogonal families of the first 7 “sounding” (radial) modeshapes (rigid-body modes are not shown) for Bowl 2, as identified from experiments. In the frequency-range explored, all the identified modes are of the $(j,0)$ type, due to the low value of the height to diameter ratio ($Z/\phi$) for Tibetan bowls, in contrast to most bells. The modal amplitudes represented are normalised to the maximum amplitude of both modes, which complicates the perception of some modeshapes. However, the spatial phase difference ($\pi/2j$) between each modal family (see section 4) is clearly seen.

Although modal frequencies and damping values were obtained from the modal identification routine, it was soon realized that the accelerometers and their cables had a non-negligible influence on the bowl modal parameters, due to the very low damping of these systems, which was particularly affected by the instrumentation.

Indeed, analysis of the near-field sound pressure time-histories, radiated by impacted bowls, showed slightly higher values for the natural frequencies and much longer decay times, when compared to those displayed after transducers were installed. Hence, we decided to use some modal parameters identified from the acoustic responses of non-instrumented impacted bowls. Modal frequencies were extracted from the sound pressure spectra and damping values were computed from the logarithm-decrement of band-pass filtered (at each mode) sound pressure decays.

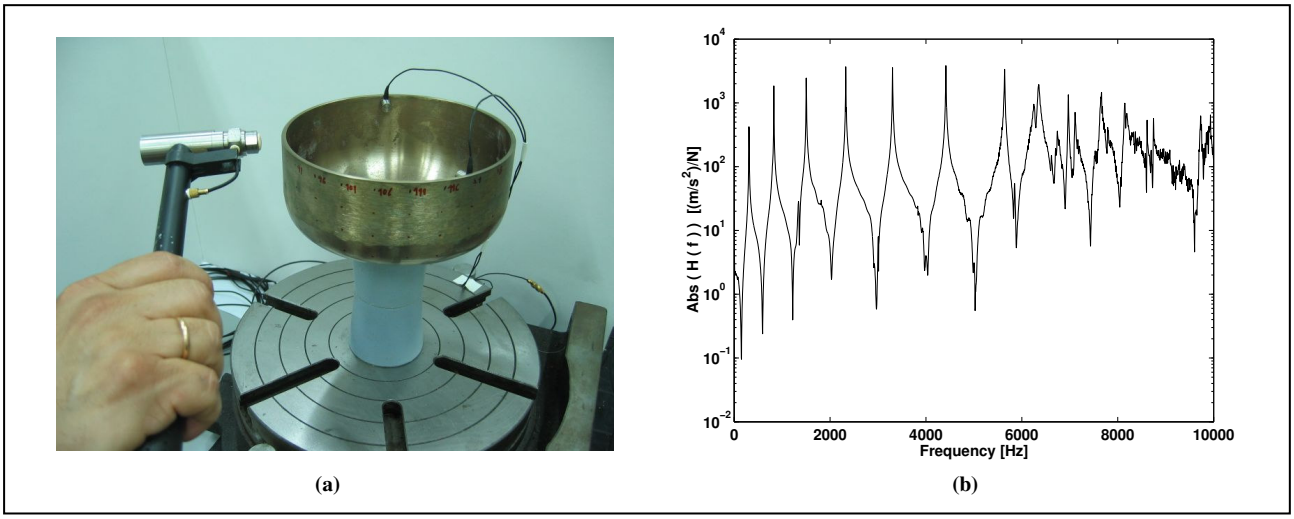


Figure 3. Experimental modal identification of Bowl 2:
(a) Picture showing the measurement grid and accelerometer locations; (b) Modulus of the accelerance frequency response function.

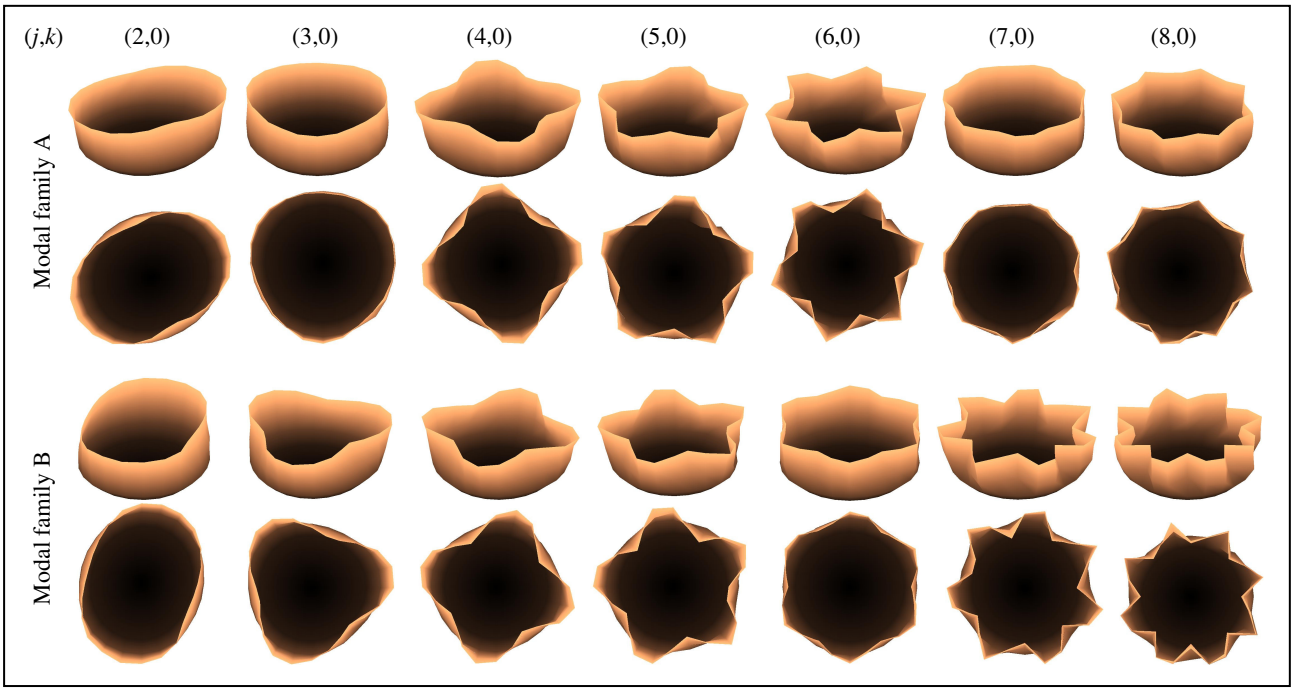


Figure 4. Perspective and top view of experimentally identified modeshapes $(j,k)$ of the first 7 elastic mode-pairs of Bowl 2 ($j$ relates to the number of nodal meridians and $k$ to the number of nodal circles – see text).

Table I – Modal frequencies and frequency ratios of bowls 1, 2 and 3 (as well as their total masses $M_T$ and rim diameters $\phi$).

| | **Bowl 1** | | | **Bowl 2** | | | **Bowl 3** | | |
|---|---|---|---|---|---|---|---|---|---|
| Total Mass | $M_T$ = 934 g | | | $M_T$ = 563 g | | | $M_T$ = 557 g | | |
| Diameter | $\phi$ = 180 mm | | | $\phi$ = 152 mm | | | $\phi$ = 140 mm | | |
| **Mode** | $f_n^A$ [Hz] | $f_n^B$ [Hz] | $f_n^{AB}/f_1^{AB}$ | $f_n^A$ [Hz] | $f_n^B$ [Hz] | $f_n^{AB}/f_1^{AB}$ | $f_n^A$ [Hz] | $f_n^B$ [Hz] | $f_n^{AB}/f_1^{AB}$ |
| (2,0) | 219.6 | 220.6 | 1 | 310.2 | 312.1 | 1 | 513.0 | 523.6 | 1 |
| (3,0) | 609.1 | 609.9 | 2.8 | 828.1 | 828.8 | 2.7 | 1451.2 | 1452.2 | 2.8 |
| (4,0) | 1135.9 | 1139.7 | 5.2 | 1503.4 | 1506.7 | 4.8 | 2659.9 | 2682.9 | 5.2 |
| (5,0) | 1787.6 | 1787.9 | 8.1 | 2328.1 | 2340.1 | 7.5 | 4083.0 | 4091.7 | 7.9 |
| (6,0) | 2555.2 | 2564.8 | 11.6 | 3303.7 | 3312.7 | 10.6 | 5665.6 | 5669.8 | 10.9 |
| (7,0) | 3427.0 | 3428.3 | 15.6 | 4413.2 | 4416.4 | 14.2 | - | - | - |
| (8,0) | 4376.3 | 4389.4 | 19.9 | 5635.4 | 5642.0 | 18.1 | - | - | - |

Table I shows the values of the double modal frequencies ( $f_n^A$ and $f_n^B$ ) of the most prominent modes of the three bowls tested, together with their ratios to the fundamental – mode (2,0) – where $f_n^{AB}$ represents the average frequency between the two modal frequencies $f_n^A$ and $f_n^B$. These values are entirely in agreement with the results obtained by Rossing [2]. Interestingly, these ratios are rather similar, in spite of the different bowl shapes, sizes and wall thickness. As rightly pointed by Rossing, these modal frequencies are roughly proportional to $j^2$, as in cylindrical shells, and inversely proportional to $\phi^2$. Rossing explains this in simple terms, something that can be also grasped from the theoretical solution for in-plane modes for rings [27]:

$$\omega_j = \frac{j(j^2-1)}{\sqrt{j^2+1}}\sqrt{\frac{EI}{\rho A R^4}}, \text{ with } j = 1,2,...,N \quad (3)$$

where $E$ and $\rho$ are the Young Modulus and density of the ring material, $I$ the area moment of inertia, $A$ the ring cross section area and $R$ the ring radius. It can be seen that as $j$ takes higher values, the first term of equation 3 tends to $j^2$, while the dependency on the ring diameter is embedded in the second term.

The frequency relationships are mildly inharmonic, which does not affect the definite pitch of this instrument, mainly dominated by the first (2,0) shell mode. As stated, dissipation is very low, with modal damping ratios typically in the range $\zeta_n$ = 0.002~0.015 % (higher values pertaining to higher-order modes). However, note that these values may increase one order of magnitude, or more, depending on how the bowls are actually supported or handled.

Further experiments were performed on the larger bowl shown in Figure 2 (Bowl 4), with $\phi$ = 262 mm, a total mass of 1533 g and a fundamental frequency of 86.7 Hz. A full modal identification was not pursued for this instrument, but ten natural frequencies were identified from measurements of the sound pressure resulting from impact tests. These modal frequencies are presented in Table II, which show a similar relation to the fundamental as the first three bowls presented in this study. For this instrument all these modes were assumed to be of the ($j$,0) type.

Table II – Modal frequencies and frequency ratios of Bowl 4.

| Mode ($j$,$k$) | $f_n$ [Hz] | $f_n/f_1$ |
|---|---|---|
| (2,0) | 86.7 | 1.0 |
| (3,0) | 252.5 | 2.9 |
| (4,0) | 490.0 | 5.7 |
| (5,0) | 788.0 | 9.1 |
| (6,0) | 1135.0 | 13.1 |
| (7,0) | 1533.0 | 17.7 |
| (8,0) | 1963.0 | 22.6 |
| (9,0) | 2429.0 | 28.0 |
| (10,0) | 2936.0 | 33.9 |
| (11,0) | 3480.0 | 40.1 |

## 4. Formulation of the dynamical system

### 4.1. Dynamical formulation of the bowl in modal coordinates

Perfectly axi-symmetrical structures exhibit double vibrational modes, occurring in orthogonal pairs with identical frequencies ( $\omega_n^A = \omega_n^B$ ) [4]. However, if a slight alteration of this symmetry is introduced, the natural frequencies of these two degenerate modal families deviate from identical values by a certain amount $\Delta\omega_n$. The use of these modal pairs is essential for the correct dynamical description of axi-symmetric bodies, under general excitation conditions. Furthermore, shell modeshapes present both radial and tangential components. Figure 5 displays a representation of the first four modeshape pairs, near the bowl rim, where the excitations are usually exerted (e.g., $z_e \approx Z$ ). Both the radial (green) and tangential (red) motion components are plotted, which for geometrically perfect bowls can be formulated as:

$$\begin{cases} \varphi_n^A(\theta) = \varphi_n^{Ar}(\theta)\,\vec{r} + \varphi_n^{At}(\theta)\,\vec{t} \\ \varphi_n^B(\theta) = \varphi_n^{Br}(\theta)\,\vec{r} + \varphi_n^{Bt}(\theta)\,\vec{t} \end{cases} \quad (4)$$

with

$$\begin{cases} \varphi_n^{Ar}(\theta) = \cos(n\theta) \\ \varphi_n^{At}(\theta) = -\sin(n\theta)/n \end{cases}; \quad \begin{cases} \varphi_n^{Br}(\theta) = \sin(n\theta) \\ \varphi_n^{Bt}(\theta) = \cos(n\theta)/n \end{cases} \quad (5,6)$$

where $\varphi_n^{Ar}(\theta)$ corresponds to the radial component of the $A$ family $n$th modeshape, $\varphi_n^{At}(\theta)$ to the tangential

component of the *A* family *n*th mode shape, etc. Figure 5 shows that spatial phase angles between orthogonal mode pairs are $\pi/2j$. One immediate conclusion can be drawn from the polar diagrams shown and equations (5,6): the amplitude of the tangential modal component decreases relatively to the amplitude of the radial component as the mode number increases. This suggests that only the lower-order modes are prone to engage in self-sustained motion due to tangential rubbing excitation by the *puja*.

If linear dissipation is assumed, the motion of the system can be described in terms of the bowl's two families of modal parameters: modal masses $m_n^X$, modal circular frequencies $\omega_n^X$, modal damping $\zeta_n^X$, and mode shapes $\varphi_n^X(\theta)$ (at the assumed excitation level $z_e \approx Z$), with $n = 1, 2, \cdots, N$, where $X$ stands for the modal family $A$ or $B$. The order $N$ of the modal truncation is problem-dependent and should be asserted by physical reasoning, supported by the convergence of computational results.

The maximum modal frequency to be included, $\omega_N$, mostly depends on the short time-scales induced by the contact parameters – all modes significantly excited by impact and/or friction phenomena should be included in the computational modal basis.

The forced response of the damped bowl can then be formulated as a set of $2N$ ordinary second-order differential equations

$$\begin{bmatrix} [M_A] & 0 \\ 0 & [M_B] \end{bmatrix} \begin{Bmatrix} \{\ddot{Q}_A(t)\} \\ \{\ddot{Q}_B(t)\} \end{Bmatrix} + \begin{bmatrix} [C_A] & 0 \\ 0 & [C_B] \end{bmatrix} \begin{Bmatrix} \{\dot{Q}_A(t)\} \\ \{\dot{Q}_B(t)\} \end{Bmatrix} + \begin{bmatrix} [K_A] & 0 \\ 0 & [K_B] \end{bmatrix} \begin{Bmatrix} \{Q_A(t)\} \\ \{Q_B(t)\} \end{Bmatrix} = \begin{Bmatrix} \{\Xi_A(t)\} \\ \{\Xi_B(t)\} \end{Bmatrix} \tag{7}$$

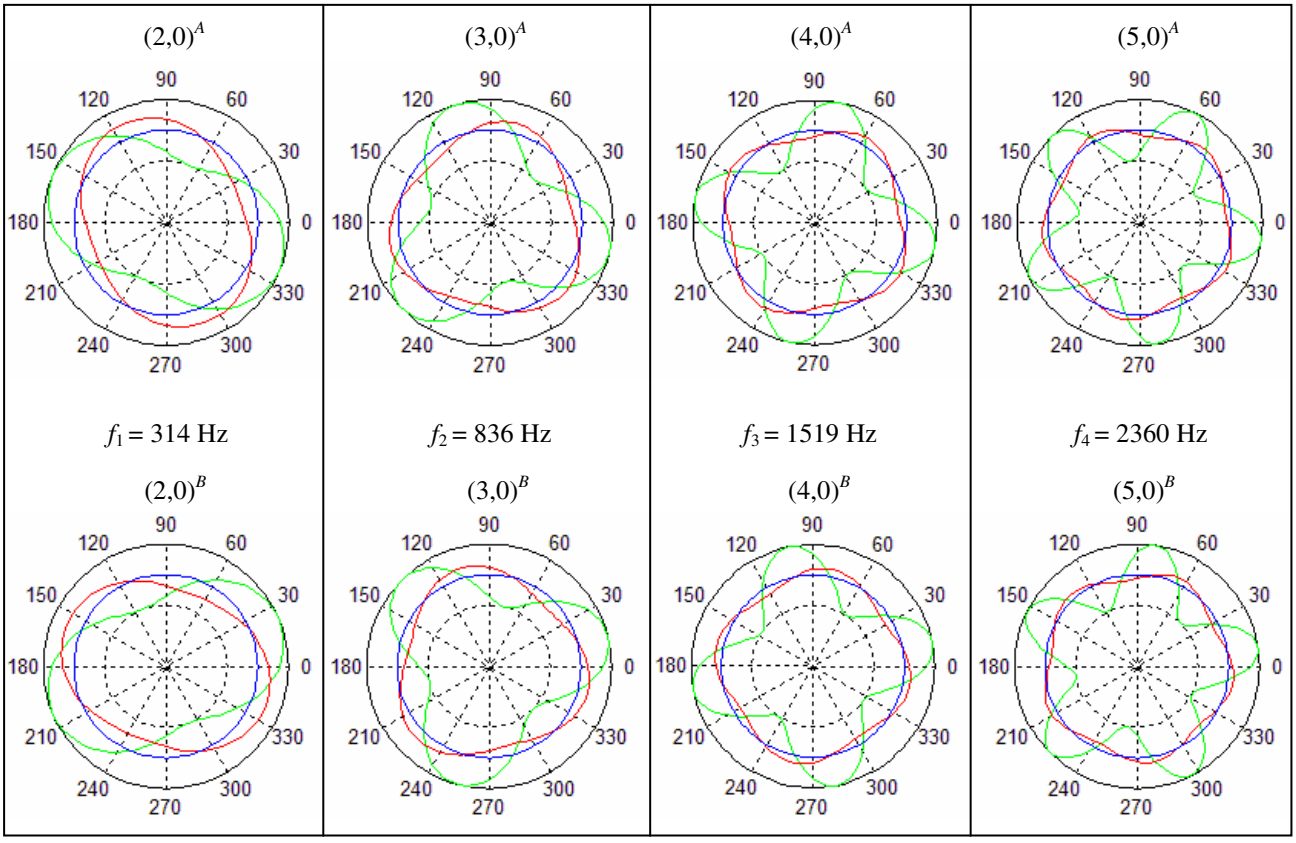


Figure 5. Mode shapes at the bowl rim of the first four orthogonal mode pairs (Blue: Undeformed; Green: Radial component; Red: Tangential component).

where:

$[M_X] = \mathrm{Diag}(m_1^X, \cdots, m_N^X)$,

$[C_X] = \mathrm{Diag}(2 m_1^X \omega_1^X \zeta_1^X, \cdots, 2 m_N^X \omega_N^X \zeta_N^X)$,

$[K_X] = \mathrm{Diag}(m_1^X (\omega_1^X)^2, \cdots, m_N^X (\omega_N^X)^2)$,

are the matrices of the modal parameters (where *X* stands for *A* or *B*), for each of the two orthogonal mode families, while $\{Q_X(t)\} = \langle q_1^X(t), \cdots, q_N^X(t) \rangle^T$ and $\{\Xi_X(t)\} = \langle \Im_1^X(t), \cdots, \Im_N^X(t) \rangle^T$ are the vectors of the modal responses and of the generalized forces, respectively. Note that, although equations (7) obviously pertain to a linear formulation, nothing prevents us from including in $\Im_n^X(t)$ all the nonlinear effects which arise from the contact/friction interaction between the bowl and the *puja*. Accordingly, the system modes become coupled by such nonlinear effects.

The modal forces $\Im_n^X(t)$ are obtained by projecting the external force field on the modal basis:

$$\Im_n^X(t) = \int_0^{2\pi} \left[ F_r(\theta,t)\, \varphi_n^{Xr}(\theta) + F_t(\theta,t)\, \varphi_n^{Xt}(\theta) \right] d\theta \qquad (8)$$

$$n = 1, 2, \cdots, N$$

where $F_r(\theta,t)$ and $F_t(\theta,t)$ are the radial (impact) and tangential (friction) force fields applied by the *puja* – e.g., a localised impact $F_r(\theta_c,t)$ and/or a travelling rub $F_{r,t}(\theta_c(t),t)$. The radial and tangential physical motions can be then computed at any location $\theta$ from the modal amplitudes $q_n^X(t)$ by superposition:

$$y_r(t) = \sum_{n=1}^{N} \left[ \varphi_n^{Ar}(\theta) \cdot q_n^A(t) + \varphi_n^{Br}(\theta) \cdot q_n^B(t) \right] \qquad (9)$$

$$y_t(t) = \sum_{n=1}^{N} \left[ \varphi_n^{At}(\theta) \cdot q_n^A(t) + \varphi_n^{Bt}(\theta) \cdot q_n^B(t) \right] \qquad (10)$$

and similarly concerning the velocities and accelerations.

### 4.2. Dynamics of the puja

As mentioned before, the excitation of these musical instruments can be performed in two basic different ways: by impact or by rubbing around the rim of the bowl with the *puja* (these two types of excitation can obviously be mixed, resulting in musically interesting effects). The dynamics of the *puja* will be formulated simply in terms of a mass $m_P$ subjected to a normal (e.g. radial) force $F_N(t)$ and an *imposed* tangential rubbing velocity $V_T(t)$ – which will be assumed constant in time for all our exploratory simulations – as well as to an initial impact velocity in the radial direction $V_N(t_0)$. These three parameters are the most relevant factors which allow the musician to play the instrument and control the mechanism of sound generation. Many distinct sounds may be obtained by changing them: in particular, $V_N(t_0) \neq 0$ with $F_N = V_T = 0$ will be "pure" impact, and $F_N(t) \neq 0$, $V_T(t) \neq 0$ with $V_N(t_0) = 0$ will be "pure" *singing* (see section 4). The radial motion of the *puja*, resulting from the external force applied and the impact/friction interaction with the bowl is given by:

$$m_P \ddot{y}_P = -F_N(t) + F_r(\theta,t) \qquad (11)$$

where $F_r(\theta,t)$ is the dynamical bowl/*puja* contact force.

### 4.3. Contact interaction formulation

The radial contact force resulting from the interaction between the *puja* and the bowl is simply modelled as a contact stiffness, eventually associated with a contact damping term:

$$F_r(\theta_c) = -K_c\, \tilde{y}_r(\theta_c,t) - C_c\, \dot{\tilde{y}}_r(\theta_c,t) \qquad (12)$$

where $\tilde{y}_r$ and $\dot{\tilde{y}}_r$ are respectively the bowl/*puja* relative radial displacement and velocity, at the (fixed or travelling) contact location $\theta_c(t)$, $K_c$ and $C_c$ are the contact stiffness and damping coefficients, directly related to the *puja* material. Other and more refined contact models – for instance of the hertzian type, eventually with hysteretic behaviour – could easily be

implemented instead of (12). Such refinements are however not a priority here.

### 4.4. Friction interaction formulation

In previous papers we have shown the effectiveness of a friction model used for the simulation of bowed bars and bowed strings [7-9, 15-18]. Such model enabled a clear distinction between sliding and adherence states, sliding friction forces being computed from the Coulomb model $F_t = -|F_r|\mu_d(\dot{\tilde{y}}_t)sgn(\dot{\tilde{y}}_t)$, where $\dot{\tilde{y}}_t$ is the bowl/*puja* relative tangential velocity, and the adherence state being modelled essentially in terms of a local "adherence" stiffness $K_a$ and some damping. We were thus able to emulate true friction sticking of the contacting surfaces, whenever $|F_t| < |F_r|\mu_s$, however at the expense of a longer computational time, as smaller integration time-steps seem to be imposed by the transitions from velocity-controlled sliding states to displacement-controlled adherence states.

In this paper, a simpler approach is taken to model friction interaction, which allows for faster computation times, although it lacks the capability to emulate true friction sticking. The friction force will be formulated as:

$$\begin{cases} F_t(\theta_c,t) = -|F_r(\theta_c,t)|\mu_d\left(\dot{\tilde{y}}_t(\theta_c,t)\right)sgn\left(\dot{\tilde{y}}_t(\theta_c,t)\right) \\ \qquad\qquad\qquad\qquad \text{, if } \left|\dot{\tilde{y}}_t(\theta_c,t)\right| \geq \varepsilon \\ F_t(\theta_c,t) = -|F_r(\theta_c,t)|\mu_s\,\dot{\tilde{y}}_t(\theta_c,t)/\varepsilon \quad \text{, if } \left|\dot{\tilde{y}}_t(\theta_c,t)\right| < \varepsilon \end{cases} \tag{13}$$

where $\mu_s$ is a "static" friction coefficient and $\mu_d(\dot{\tilde{y}}_t)$ is a "dynamic" friction coefficient, which depends on the *puja*/bowl relative surface velocity $\dot{\tilde{y}}_t$. We will use the following model:

$$\mu_d(\dot{\tilde{y}}_t) = \mu_\infty + (\mu_s - \mu_\infty)\exp\left(-C\left|\dot{\tilde{y}}_t(\theta_c,t)\right|\right) \tag{14}$$

where, $0 \leq \mu_\infty \leq \mu_s$ is an asymptotic lower limit of the friction coefficient when $\left|\dot{\tilde{y}}_t\right| \to \infty$, and parameter $C$ controls the decay rate of the friction coefficient with the relative sliding velocity, as shown in the typical plot of Figure 6(a). This model can be fitted to the available experimental friction data (obtained under the assumption of instantaneous velocity-dependence), by adjusting the empirical constants $\mu_s$, $\mu_\infty$ and $C$.

Notice that both equations (13) correspond to velocity-controlled friction forces. For values of $\dot{\tilde{y}}_t$ outside the interval $[-\varepsilon,\varepsilon]$, the first equation simply states Coulomb's model for sliding. Inside the interval $[-\varepsilon,\varepsilon]$, the second equation models a state of *pseudo-adherence* at very low tangential velocities. Obviously, $\varepsilon$ acts as a regularization parameter for the friction force law, replacing the "zero-velocity" discontinuity (which renders the adherence state numerically tricky), as shown in Figure 6(b). This regularization method, extensively developed in [28], has been often used as a pragmatic way to deal with friction phenomena in the context of dynamic problems. However, using this model, the friction force will always be zero at zero sliding velocity, inducing a relaxation on the "adherence" state (dependent on the magnitude of $\varepsilon$), and therefore disabling a true sticking behaviour. How pernicious this effect may be is problem-dependent – systems involving a prolonged adherence will obviously suffer more from the relaxation effect than systems which are sliding most of the time. For the problem addressed here, we have obtained realistic results using formulation (13), for small enough values of the regularization domain (we used $\pm\varepsilon \approx 10^{-4}\,\text{ms}^{-1}$) – results which do not seem to critically depend on $\varepsilon$, within reasonable limits.

### 4.5. Time-step integration

For given external excitation and initial conditions, the previous system of equations is numerically integrated using an adequate time-step algorithm. Explicit integration methods are well suited for the contact/friction model developed here. In our implementation, we used a simple Velocity-Verlet integration algorithm [29], which is a low-order explicit scheme.

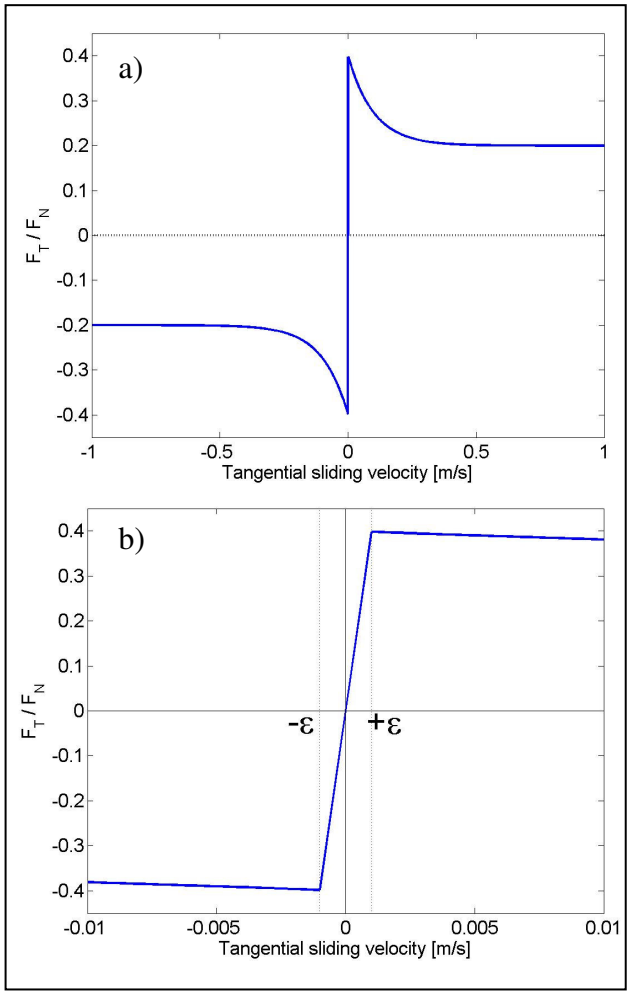


Figure 6. Friction coefficient as a function of the contact relative tangential velocity ( $\mu_\infty = 0.2$, $\mu_s = 0.4$, $C = 10$): (a) For -1< $\tilde{\dot{y}}_t$ <1; (b) For -0.01< $\tilde{\dot{y}}_t$ <0.01.

## 5. Numerical simulations

The numerical simulations presented here are based on the modal data of two different sized instruments: Bowl 2 and Bowl 4, which were identified in section 2. The simulations based on the smaller instrument data will be used to highlight the main features of the dynamics of these instruments, while the larger instrument simulations will serve the purpose of studying the influence of the contact/friction parameters on the oscillation regimes.

The *puja* is modeled as a simple mass of 20 g, moving at tangential velocity $V_T$, and subjected to an external normal force $F_N$ as well as to the bowl/*puja* nonlinear interaction force. We explore a significant range of rubbing parameters: $F_N = 1 \sim 9$ N and $V_T = 0.1 \sim 0.5$ m/s, which encompass the usual playing conditions, although calculations were made also using impact excitation only. For clarity, the normal force and tangential velocity will be assumed time-constant, in the present simulations. However, nothing would prevent us from imposing any time-varying functions $F_N(t)$ and $V_T(t)$, or even – as musicians would do – to couple the generation of $F_N(t)$ and $V_T(t)$ with the nonlinear bowl/*puja* dynamical simulation, through well-designed control strategies, in order to achieve a suitable response regime.

The contact model used in all rubbing simulations of Bowl 2 has a contact stiffness of $K_c = 10^6$ N/m and a contact dissipation of $C_c = 50$ Ns/m, which appear adequate for the present system. However, concerning impact simulations of this instrument, contact parameters ten times higher and lower were also explored. The friction parameters used in numerical simulations of this instrument are $\mu_s = 0.4$, $\mu_\infty = 0.2$ and $C = 10$ (see Figure 6). In relation to the numerical simulations of Bowl 4, different contact/friction parameters were used to simulated friction by *pujas* made of different materials, namely rubber and wood. Its values will be described in section 5.4.

In section 4.1 a few general remarks were produced concerning the order of the modal basis to use. With respect to the present system, the choice of the modal basis order of truncation is not difficult and certainly not critical, as only a few modes are excited (in contrast with bowed strings). For easily understandable physical reasons, modes with modal stiffness much higher than the contact stiffness are not significantly excited, so a reasonable criterion to choose a minimum order of truncation $N$ is to compare $K_c$ with the successive $K_n$ of the modal series. In the present study a maximum value of $K_c = 10^6$ N/m is used, then it is reasonable to assume that modes with $K_n$ much higher than $10^7$ N/m will be "useless". For Bowl 2, we decided to use seven mode pairs, the maximum value $K_N$ being of the order $K_{2\times7} \sim 10^8$ N/m. Indeed, this is a generous modal basis, and four mode pairs would do equally well, as $K_{2\times4} \sim 10^7$ N/m. However it is pointless to discuss on such a detail, when the number of modes is low. In relation to the larger Bowl 4, ten mode pairs were used, following the same reasoning. Both computational and experimental results confirm that the truncation criterion adopted is adequate.

As discussed before, assuming a perfectly symmetrical bowl, simulations were performed using identical frequencies for each mode-pair ($\omega_n^A = \omega_n^B$). However, a few computations were also performed for less-than-perfect systems, asymmetry being then modelled introducing a difference (or "split") $\Delta\omega_n$ between the frequencies of each mode pair. An average value of 0.005% was used for all modal damping coefficients. In order to cope with the large settling times that arise with singing bowls, 20 seconds of computed data were generated (enough to accommodate transients for all rubbing conditions), at a sampling frequency of 22050 Hz.

### 5.1. Impact responses

Figures 7(a, b) display the simulated responses of a perfectly symmetrical bowl to an impact excitation ($V_N(t_0)$=1 m/s), assuming different values for the contact model parameters. The time-histories of the response displacements pertain to the impact location. The spectrograms are based on the corresponding velocity responses. Typically, as the contact stiffness increases from $10^5$ N/m to $10^7$ N/m, higher-order modes become increasingly excited and resonate longer. The corresponding simulated sounds become progressively brighter, denoting the "metallic" bell-like tone which is clearly heard when impacting real bowls using wood or metal *pujas*.

### 5.2. Friction-excited responses

Figure 8 shows the results obtained when rubbing a perfectly symmetrical bowl near the rim, using fairly standard rubbing conditions: $F_N = 3$ N and $V_T = 0.3$ m/s. The plots shown pertain to the following response locations: (a) the travelling contact point between the bowl and the *puja*; (b) a fixed point in the bowl's rim. Depicted are the time-histories and corresponding spectra of the radial (green) and tangential (red) displacement responses, as well as the spectrograms of the radial velocity responses.

As can be seen, an instability of the first "elastic" shell mode (with 4 azimuthal nodes) arises, with an exponential increase of the vibration amplitude until saturation by nonlinear effects is reached (at about 7.5 s), after which the self-excited vibratory motion of the bowl becomes steady. The response spectra show that most of the energy lays in the first mode, the others being marginally excited. Notice the dramatic differences between the responses at the travelling contact point and at a fixed location. At the moving contact point, the motion amplitude does not fluctuate and the tangential component of the motion is significantly higher than the radial component. On the contrary, at a fixed location, the motion amplitude fluctuates at a frequency which can be identified as being four times the spinning frequency of the *puja*: $\Omega_{fluct} = 4\Omega_{puja} = 4\left(2V_T/\phi\right)$. Furthermore, at a fixed location, the amplitude of the radial motion component is higher than the tangential component.

The animations of the bowl and *puja* motions enable an interpretation of these results. After synchronisation of the self-excited regime, the combined responses of the first mode-pair result in a vibratory motion according to the 4-node modeshape, which however spins, "following" the revolving *puja*. Furthermore, synchronisation settles with the *puja* interacting near a node of the radial component, corresponding to an anti-nodal region of the tangential component – see Figure 5 and Equations (5,6). In retrospect, this appears to make sense – indeed, because of the friction excitation mechanism in singing bowls, the system modes self-organize in such way that a high *tangential* motion-component will arise at the contact point, where energy is inputted.

At any fixed location, a transducer will "see" the vibratory response of the bowl modulated in amplitude, as the 2*j* alternate nodal and anti-nodal regions of the "singing" modeshape revolve. For a listener, the rubbed bowl behaves as a spinning quadropole – or, in general, a 2*j*-pole (depending on the self-excited mode *j*) – and the radiated sound will always be perceived with beating phenomena, even for a perfectly symmetrical bowl. Therefore the sound files available were generated from the velocity time-history at a fixed point in the bowl rim.

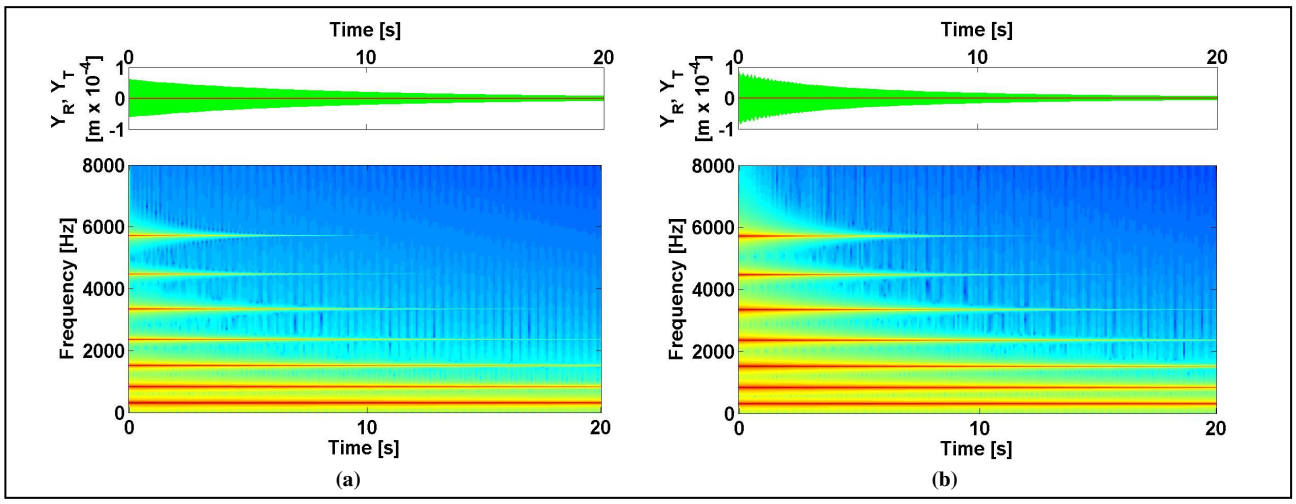


Figure 7. Displacement time histories (top) and spectrograms (bottom) of the response of Bowl 2 to impact excitation with two different values of the bowl/*puja* contact stiffness: (a) $10^5$ N/m (sound file available); (b) $10^7$ N/m (sound file available).

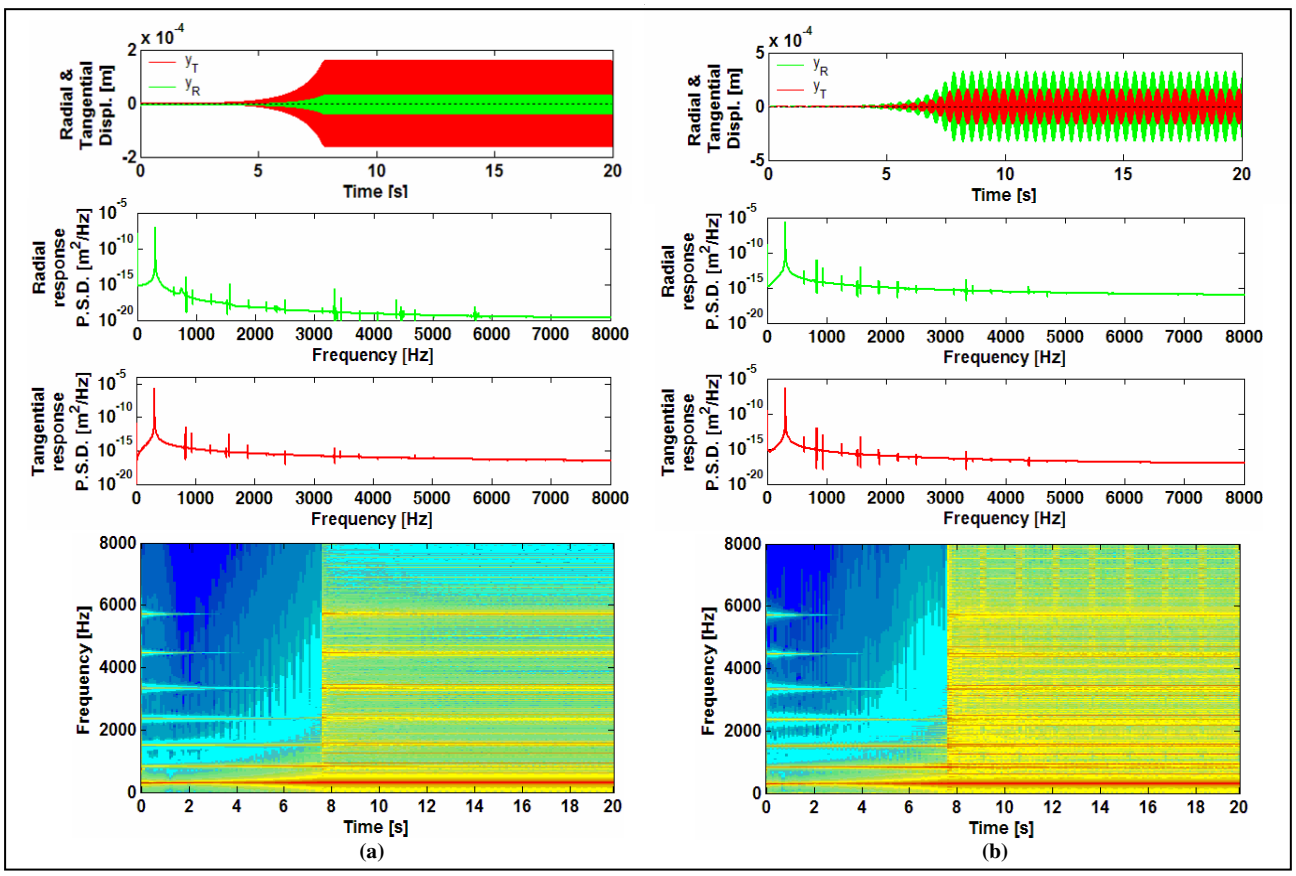


Figure 8. Time-histories, spectra and spectrograms of the dynamical response of Bowl 2 to friction excitation when $F_N = 3$ N, $V_T = 0.3$ m/s: (a) at the bowl/*puja* travelling contact point; (b) at a fixed point of the bowl rim (sound file available).

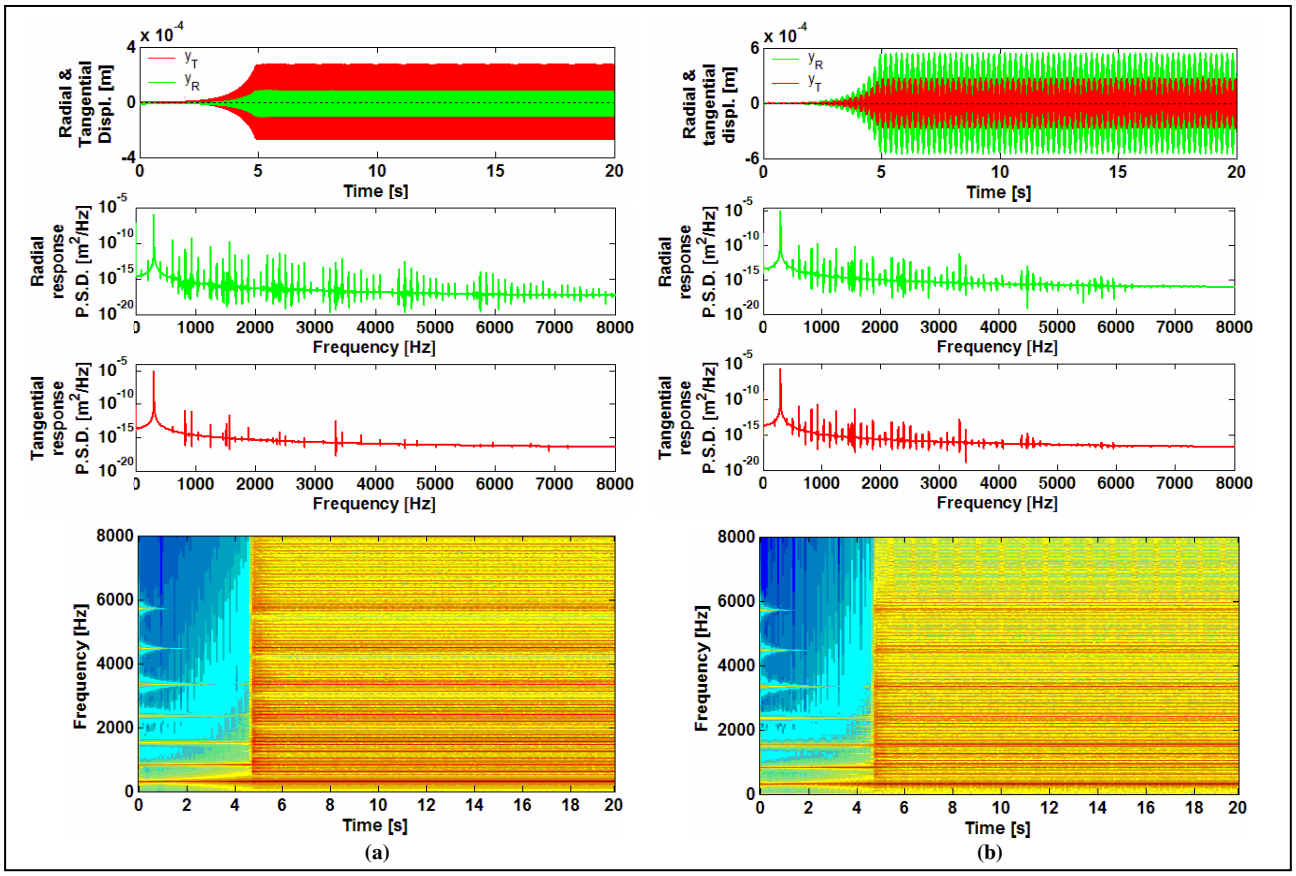


Figure 9. Time-histories, spectra and spectrograms of the dynamical response of Bowl 2 to friction excitation when $F_N = 7$ N, $V_T = 0.5$ m/s: (a) at the bowl/*puja* travelling contact point; (b) at a fixed point of the bowl rim (sound file available).

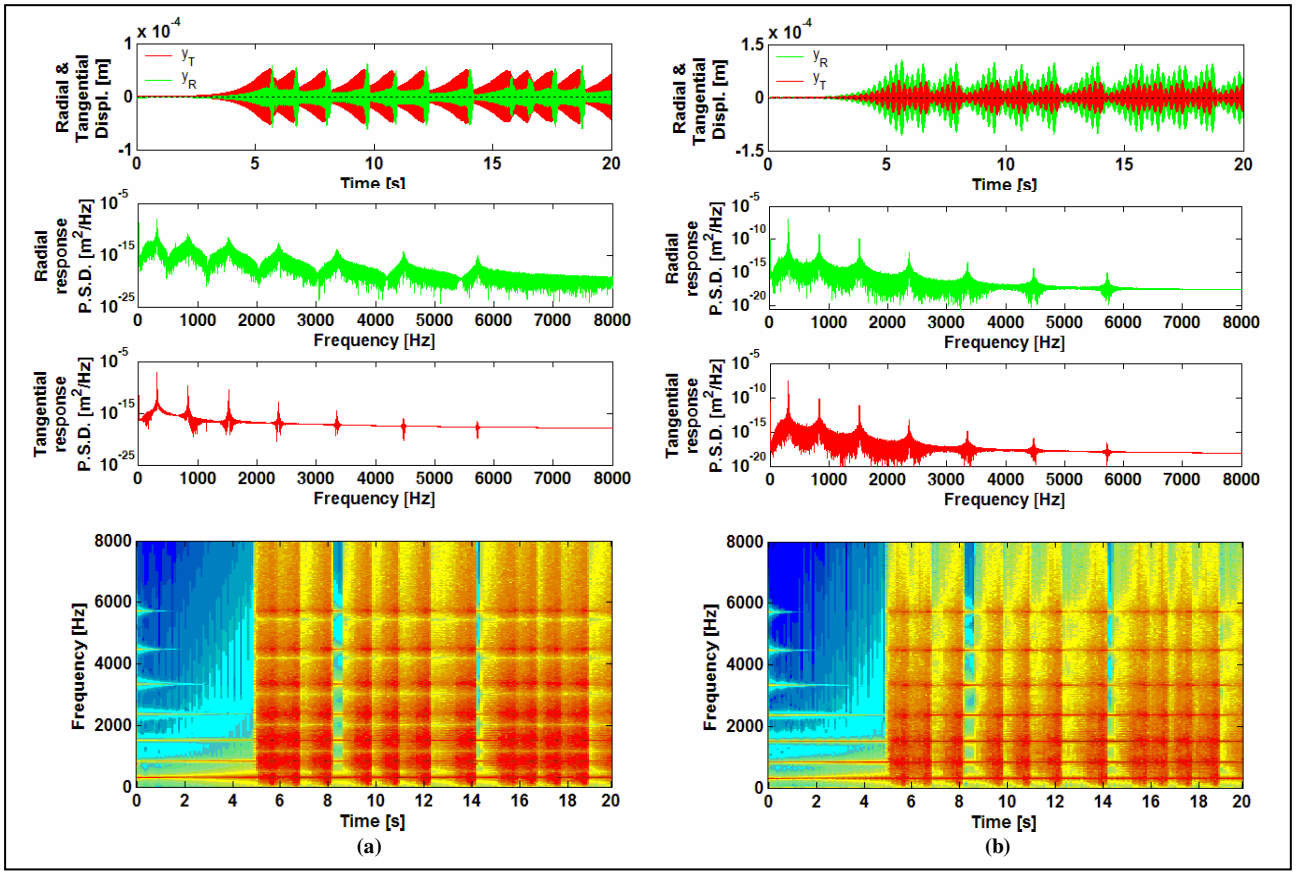


Figure 10. Time-histories, spectra and spectrograms of the dynamical response of Bowl 2 to friction excitation when $F_N = 1$ N, $V_T = 0.5$ m/s: (a) at the bowl/*puja* travelling contact point; (b) at a fixed point of the bowl rim (sound file available).

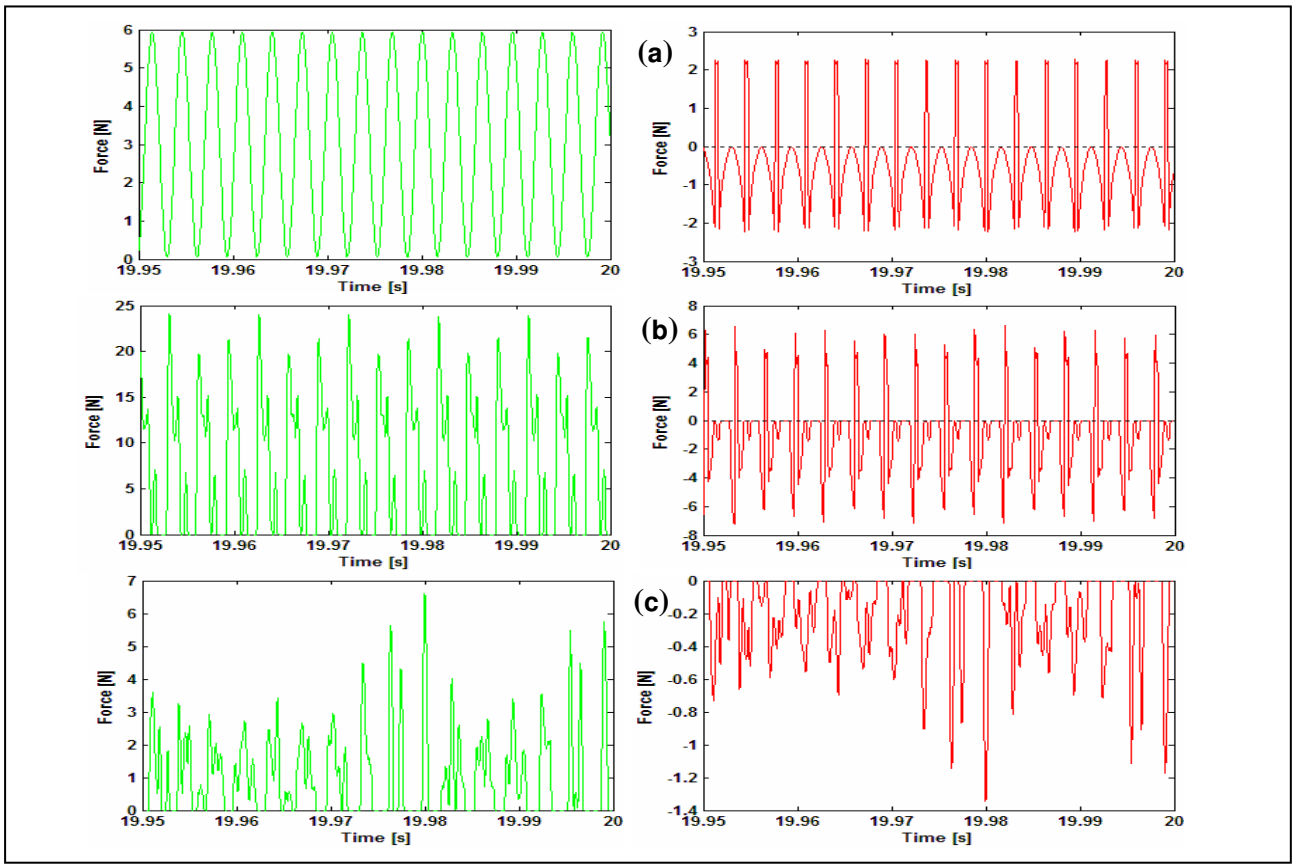


Figure 11. Radial (green) and tangential (red) interaction forces between the bowl and the travelling *puja*: (a) $F_N = 3$ N, $V_T = 0.3$ m/s; (b) $F_N = 7$ N, $V_T = 0.5$ m/s; (c) $F_N = 1$ N, $V_T = 0.5$ m/s.

Following the previous remarks, the out-of-phase envelope modulations of the radial and tangential motion components at a fixed location, as well as their amplitudes, can be understood. Indeed, all necessary insight stems from Equations (5,6) and the first plot of Figure 5.

In order to confirm the rotational behaviour of the self-excited mode we performed a simple experiment under normal playing (rubbing) conditions on Bowl 2. The near-field sound pressure radiated by the instrument was recorded by a microphone at a fixed point, approximately 5 cm from the bowl's rim. While a musician played the instrument, giving rise to a self-sustained oscillation of the first shell mode ($j$ = 2, see Figures 4 and 5), the position of the rotating puja was monitored by an observer which emitted a short impulse at the puja passage by the microphone position. Since sound radiation is mainly due to the radial motion of the bowl, the experiment proves the existence of a radial vibrational nodal region at the travelling point of excitation. Between each two passages of the puja by this point (i.e. one revolution), 4 sound pressure maxima are recorded, corroborating our previous comments that the listener hears a beating phenomena (or pseudo-beating) originating from a rotating 2$j$-pole source, whose "beating-frequency" is proportional to the revolving frequency of the puja. Such behaviour will be experimentally documented in section 5.4.

It should be noted that our results basically support the qualitative remarks provided by Rossing, when discussing friction-excited musical glass-instruments (see [4] or his book [2] pp. 185-187, the only references, to our knowledge, where some attention has been paid to these issues). However, his main point "*The location of the maximum motion follows the moving finger around the glass*" may now be further clarified: the "maximum motion" following the exciter should refer in fact to the maximum *tangential* motion component (and not the radial component, as might be assumed).

Before leaving this example, notice in Figure 11(a) the behaviour of the radial and tangential components of the bowl/*puja* contact force, on several cycles of the steady motion. The radial component oscillates between almost zero and the double of the value $F_N$ imposed to the *puja*, and contact is never disrupted. The plot of the friction force shows that the bowl/*puja* interface is sliding during most of the time. This behaviour is quite similar to what we observed in simulations of bowed bars, and is in clear contrast to bowed strings, which adhere to the bow during most of the time – see [9], for a detailed discussion. The fact that sticking only occurs during a short fraction of the motion, justifies the simplified friction model which has been used for the present computations.

Figure 9 shows the results for a slightly different regime, corresponding to rubbing conditions: $F_N = 7$ N and $V_T = 0.5$ m/s . The transient duration is smaller than in the previous case (about 5 s). Also, because of the higher tangential *puja* velocity, beating of the vibratory response at the fixed location also displays a higher frequency. This motion regime seems qualitatively similar to the previous example, however notice that the response spectra display more energy at higher frequencies, and that is because the contact between the exciter and the bowl is periodically disrupted, as shown in the contact force plots of Figure 11(b). One can see that, during about 25% of the time, the contact force is zero. Also, because of moderate impacting, the maxima of the radial component reach almost $3\,F_N$. Both the radial and friction force components are much less regular than in the previous example, but this does not prevent the motion from being nearly-periodic.

Figure 10 shows a quite different behaviour, when $F_N = 1$ N and $V_T = 0.5$ m/s . Here, a steady motion is never reached, as the bowl/*puja* contact is disrupted whenever the vibration amplitude reaches a certain level. As shown in Figure 11 (c), severe chaotic impacting arises (the amplitude of the radial component reaches almost $7\,F_N$ ), which breaks the mechanism of energy transfer, leading to a sudden decrease of the motion amplitude. Then, the motion build-up starts again until the saturation level is reached, and so on. As can be expected, this intermittent response regime results in

curious sounds, which interplay the aerial characteristics of "singing" with a distinct "ringing" response due to chaotic chattering. Anyone who ever attempted to play a Tibetan bowl is well aware of this sonorous saturation effect, which can be musically interesting, or a vicious nuisance, depending on the context.

To get a clearer picture of the global dynamics of this system, Figures 12 and 13 present the domains covered by the three basic motion regimes (typified in Figures 8-10), as a function of $F_N$ and $V_T$: (1) Steady self-excited vibration with permanent contact between the *puja* and the bowl (green data); (2) Steady self-excited vibrations with periodic contact disruption (yellow data); (3) Unsteady self-excited vibrations with intermittent amplitude increasing followed by attenuation after chaotic chattering (orange data). Note that, under different conditions, the self-excitation of a different mode may be triggered – for instance, by starting the vibration with an impact followed by rubbing. Such issue will be discussed later on this paper.

Figure 12(a) shows how the initial transient duration depends on $F_N$ and $V_T$. In every case, transients are shorter for increasing normal forces, though such dependence becomes almost negligible at higher tangential velocities. At constant normal force, the influence of $V_T$ strongly depends on the motion regime. Figure 12 (b) shows the fraction of time with motion disruption. It is obviously zero for regime (1), and growing up to 30 % at very high excitation velocities. It is clear that the "ringing" regime (3) is more prone to arise at low excitation forces and higher velocities.

Figures 13(a) and (b) show the root-mean-square vibratory amplitudes *at the traveling contact point*, as a function of $F_N$ and $V_T$. Notice that the levels of the radial components are much lower than the corresponding levels of the tangential component, in agreement with the previous comments. These plots show some dependence of the vibratory level on the response regime. Overall, the vibration amplitude increases with $V_T$ for regime (1) and decreases for regime (3). On the other hand, it is almost independent of $F_N$ for regime (1), while it increases with $F_N$ for regime (3).

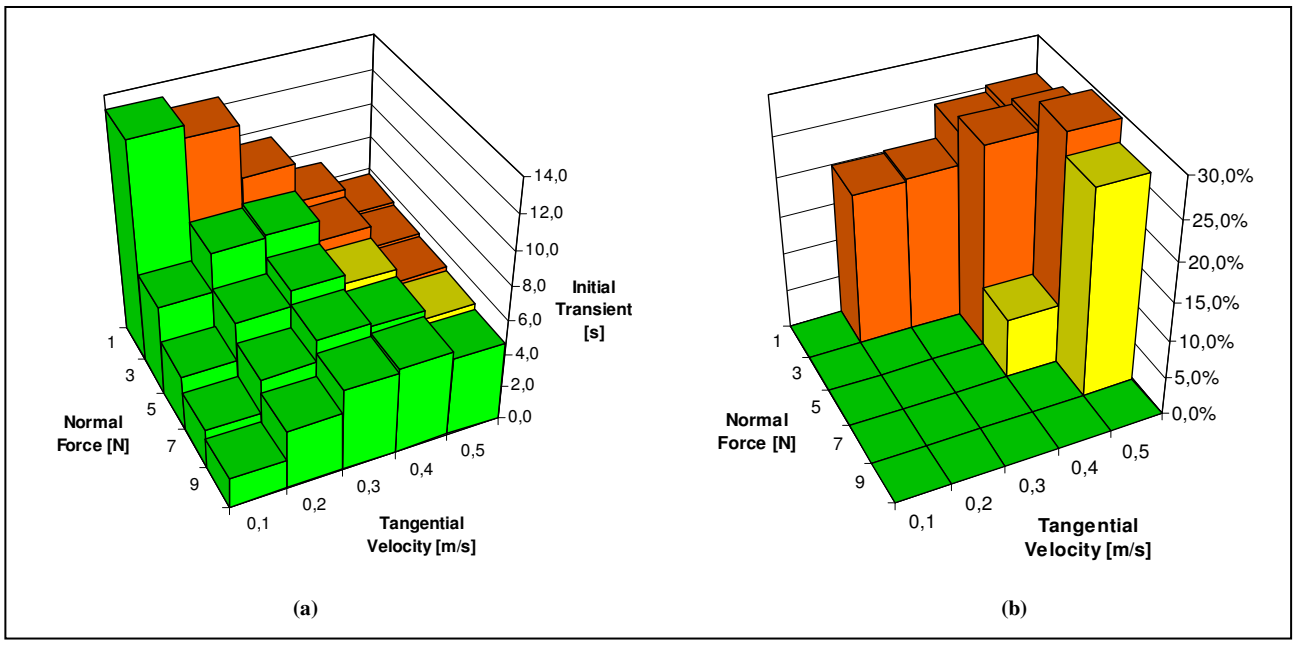


Figure 12. (a) Initial transient duration and (b) percentage of time with no bowl/*puja* contact, as a function of $F_N$ and $V_T$.

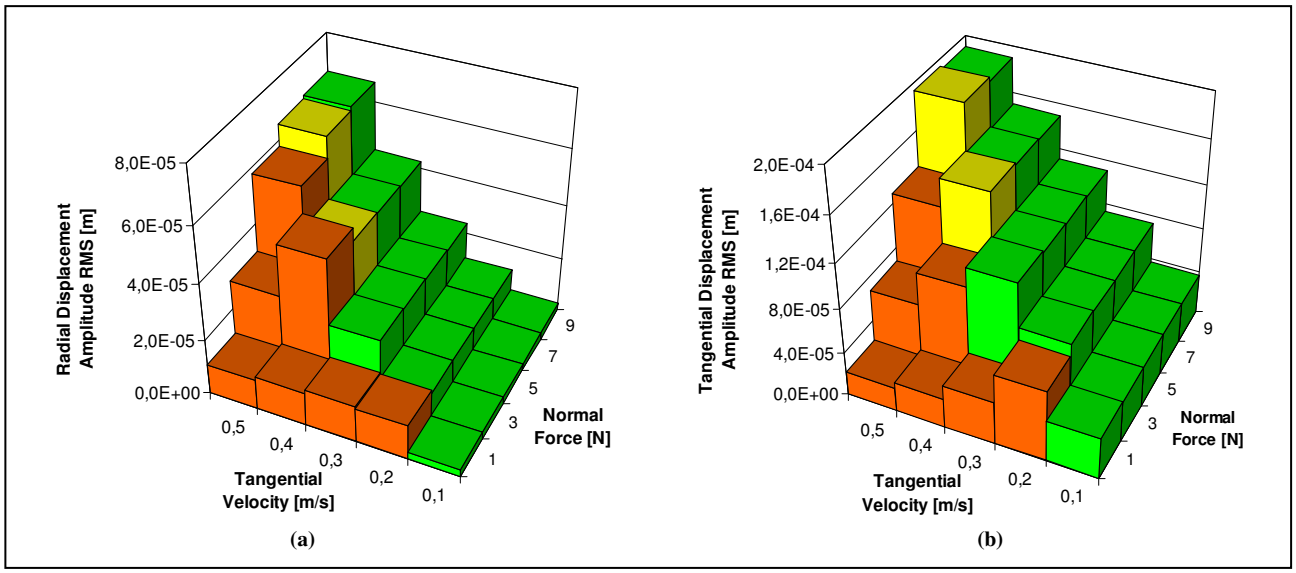


Figure 13. Displacement amplitude (RMS) at the bowl/*puja* travelling contact point, as a function of $F_N$ and $V_T$: (a) Radial motion component; (b) Tangential motion component.

### 5.3. Non-symmetrical bowls

Figures 14(a) and (b) enable a comparison between the impact responses of perfectly symmetrical and a non-symmetrical bowls. Here, the lack of symmetry has been simulated by introducing a frequency split of 2% between the frequencies of each mode-pair (e.g. $\Delta\omega_n = 0.02\omega_n$), all other aspects remaining identical – such crude approach is adequate for illustration purposes.

Notice that the symmetrical bowl only displays radial motion *at the impact point* (as it should), while the unsymmetrical bowl displays both radial and tangential motion components due to the different propagation velocities of the travelling waves excited. On the other hand, one can notice in the response spectra of the unsymmetrical system the frequency-split of the various mode-pairs. This leads to beating of the vibratory response, as clearly seen on the corresponding spectrogram.

Figure 15 shows the self-excited response of the symmetrical bowl, when rubbed at $F_N = 3$ N and $V_T = 0.3$ m/s. Notice that sound beating due to the spinning of the response modeshape dominates, when compared to effect of modal frequency-split. Interestingly, the slight change in the modal frequencies was enough to modify the nature of the self-excited regime, which went from type (1) to type (3). This fact shows the difficulties in mastering these apparently simple instruments.

### 5.4. Influence of the contact/friction parameters

Playing experience shows that rubbing with *pujas* made of different materials may trigger self-excited motions at different fundamental frequencies. This suggests that friction and contact parameters have an important influence on the dynamics of the bowl regimes. Although this behaviour was present in all the bowls used in this study, it was clearly easier to establish these different regimes on a larger bowl. Therefore we illustrate the different behaviours that can be obtained, by using Bowl 4 and parameters corresponding to two *pujas*, respectively covered with rubber and made of naked wood.

As the frequency separation between mode-pairs was relatively small for this bowl, we assume a perfectly symmetrical bowl, and performed simulations using 10 mode-pairs with identical frequencies ($\omega_n^A = \omega_n^B$) – see Table II. An average value of 0.005% was used for all modal damping coefficients. In order to cope with the large settling times that arise with singing bowls, 30 seconds of computed data were generated (enough to accommodate transients for all rubbing conditions).

Figure 16 shows a computed response obtained when using a soft *puja* with relatively high friction. Here a contact stiffness $K_c = 10^5$ N/m was used, assuming friction parameters $\mu_s = 0.8$, $\mu_\infty = 0.4$ and $C = 10$, under playing conditions $F_N = 5$ N and $V_T = 0.3$ m/s.

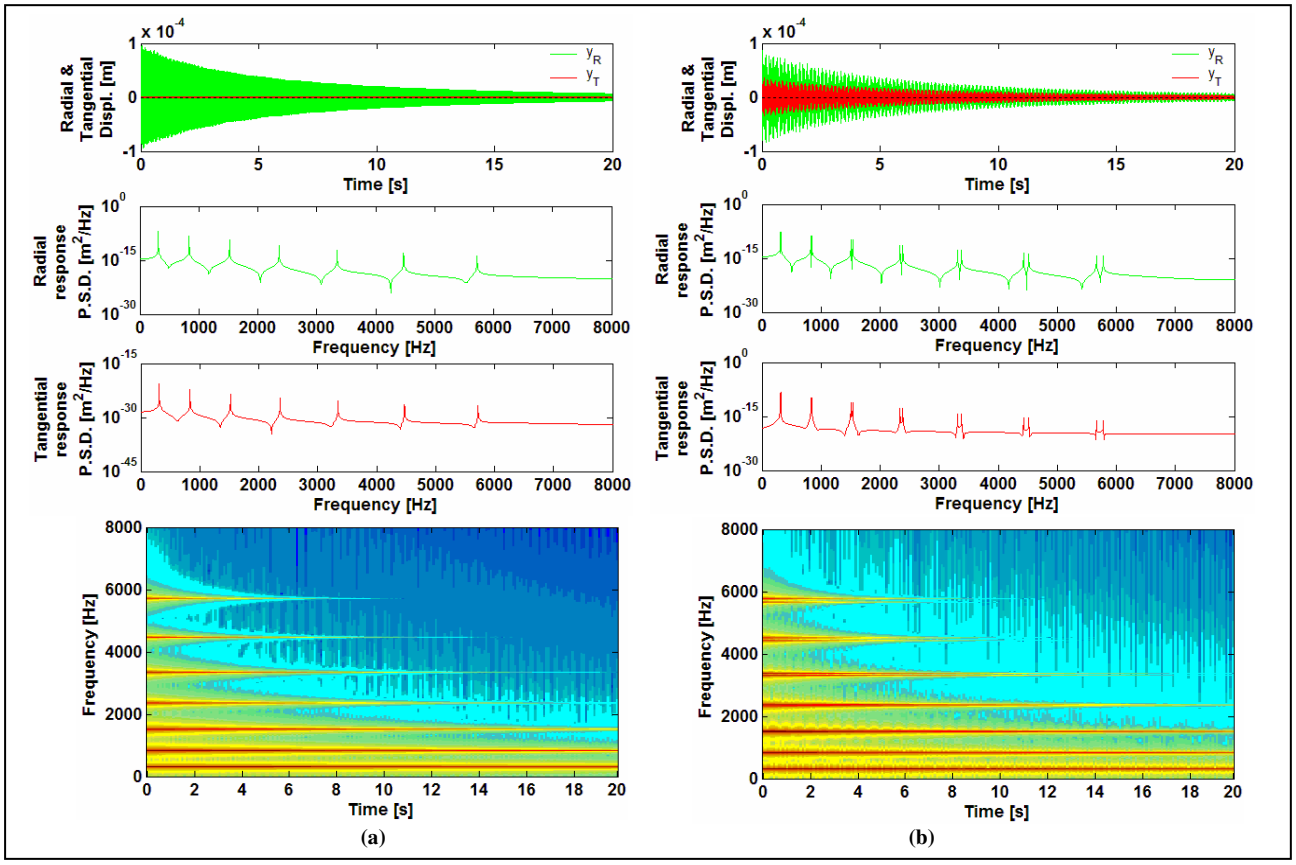


Figure 14. Dynamical responses of an impacted bowl, at the impact location:
(a) Axi-symmetrical bowl (0% frequency split); (b) Non-symmetrical bowl with 2% frequency split (sound file available).

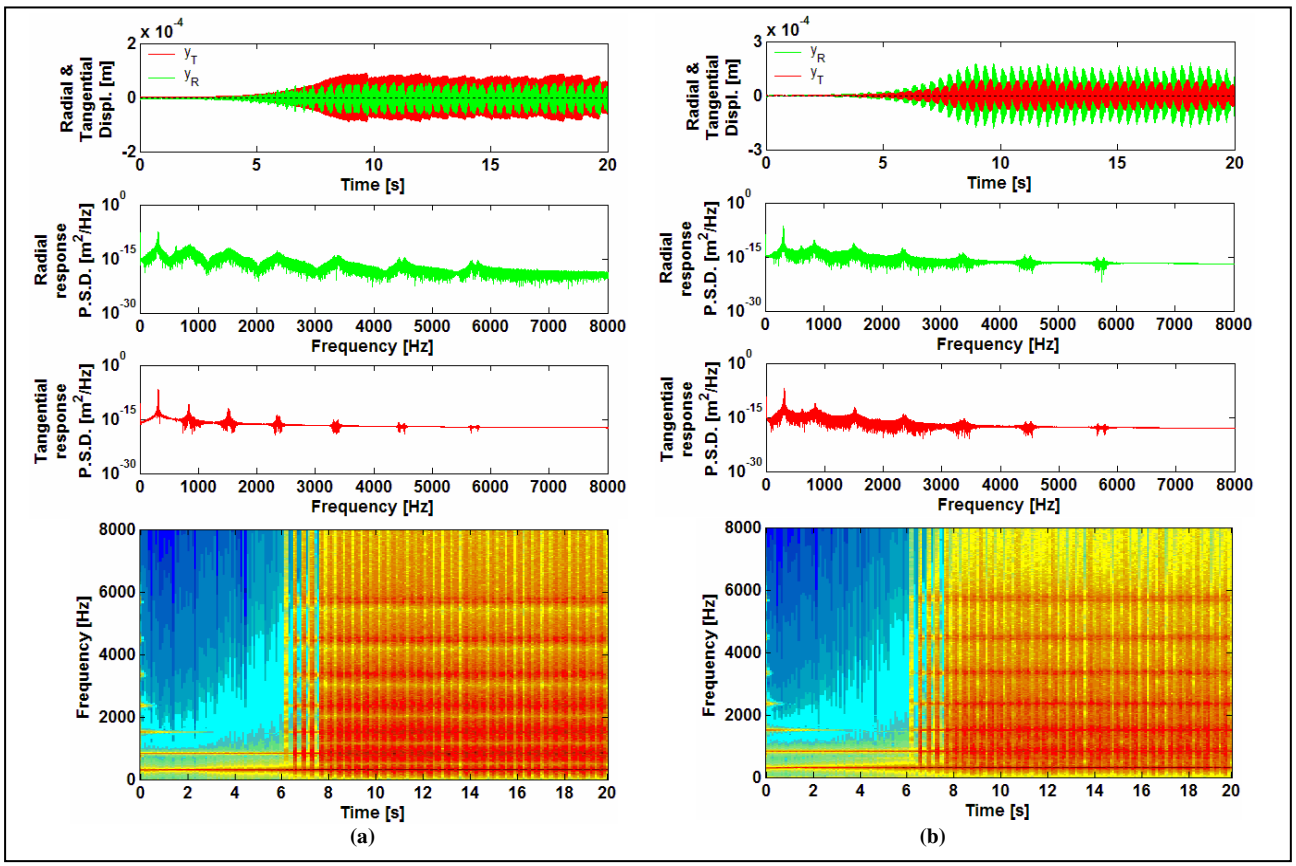


Figure 15. Dynamical response of a rubbed bowl with 2% frequency split when $F_N = 3$ N, $V_T = 0.3$ m/s:
(a) at the bowl/*puja* travelling contact point; (b) at a fixed point of the bowl rim (sound file available).

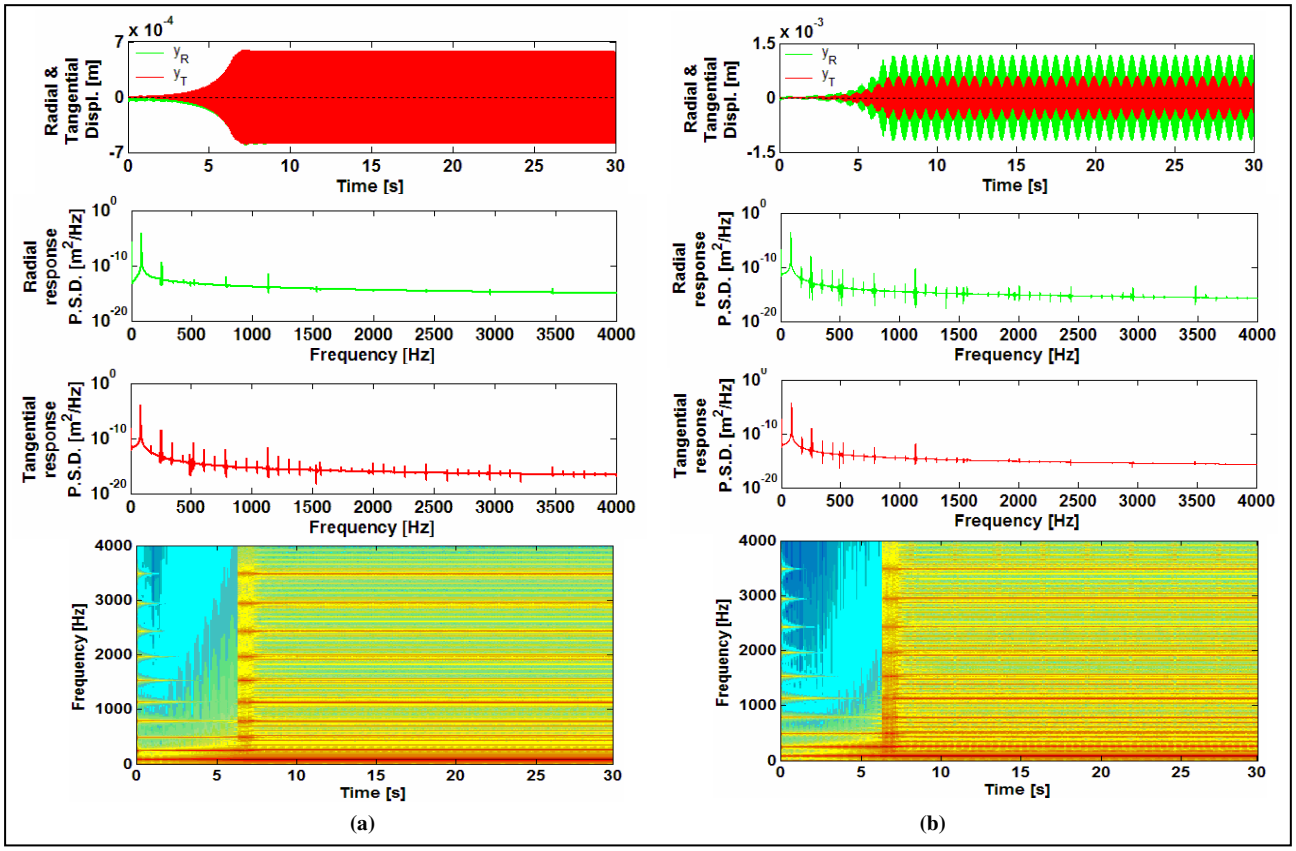


Figure 16. Time-histories, spectra and spectrograms of the dynamical response of Bowl 4 excited by a rubber-covered *puja* for $F_N = 5$ N and $V_T = 0.3$ m/s: (a) at the bowl/*puja* travelling contact point; (b) at a fixed point of the bowl rim (sound file available).

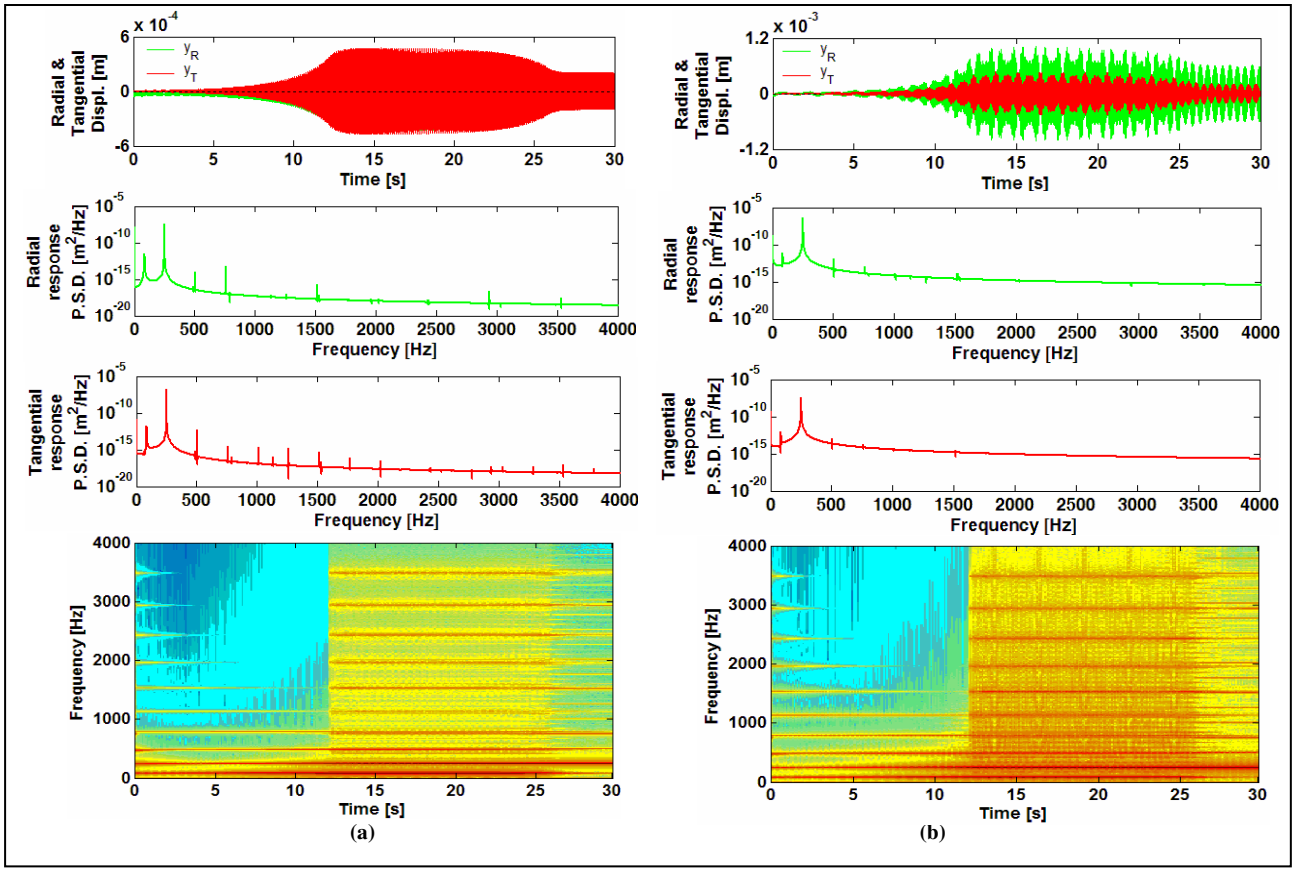


Figure 17. Time-histories, spectra and spectrograms of the dynamical response of Bowl 4 excited by a wooden *puja* for $F_N = 5$ N and $V_T = 0.3$ m/s: (a) at the bowl/*puja* travelling contact point; (b) at a fixed point of the bowl rim (sound file available).

The plot shown in *a)* displays the radial (green) and tangential (red) bowl motions at the *travelling* contact point with the puja. These are of about the same magnitude, and perfectly steady as soon as the self-excited motion locks-in. In contrast, plot *b)* shows that the radial motion clearly dominates when looking at a *fixed* location in the bowl, with maximum amplitudes exceeding those of the travelling contact point by a factor two. Most important, beating phenomena is observed at a frequency related to the puja spinning frequency $\Omega_p = 2V_T/\phi$, as also observed in relation to Bowl 2. The spectrum shown in plot *c)* presents the highest energy near the first modal frequency, while the spectrogram *d)* shows that the motion settles after about 7 seconds of exponential divergence. Indeed, our computed animations show that the unstable first bowl mode ($\approx 87$Hz) spins, following the *puja* motion, with the contact point located near one of the four nodes of the excited modeshape (see Figure 4). The bowl radiates as a quadro-pole spinning with frequency $\Omega_p$, and beating is perceived with frequency $\Omega_{beat} = 4\Omega_p$.

Figure 17 shows a computed response obtained when using a harder puja with lower friction, assuming $K_c = 10^6$ N/m, $\mu_s = 0.4$ and $\mu_\infty = 0.2$, under the same playing conditions as before.

The self-excited motion takes longer to emerge and is prone to qualitative changes. However, vibration is essentially dominated by the *second* modal frequency ($\approx 253$Hz), with a significant contribution of the first mode during the initial 25 seconds. This leads to more complex beating phenomena, except during the final 5 seconds of the simulation, where one can notice that, in spite of the similar value of $V_T$ used, beating is at a higher frequency than in Figure 16. Indeed, because the second elastic mode is now unstable (see Figure 4), the bowl radiates as a hexa-pole spinning with frequency $\Omega_p$, and beating is perceived with frequency $\Omega_{beat} = 6\Omega_p$.

Figure 18(a) shows the experimental results recorded by a microphone placed near the bowl rim, while playing with a *rubber-covered* puja. As described before, timing pulses were generated at each consecutive revolution, when the puja and microphone were nearby. Vibration was dominated by an instability of the *first* mode (2,0) and, in spite of mildly-controlled human playing, it is clear that radiation is minimal near the contact point and that four beats per revolution are perceived. When a harder *naked wood* puja was used, the initial transient became longer, before an instability of the *second* mode (3,0) settled. The bowl responses tended to be less regular, as shown in Figure 18(b), however six beats per revolution are clearly perceived. All these features support the simulation results presented in Figures 16 and 17, as well as the physical discussion presented in section 5.2.

The present results stress the importance of the contact/friction parameters, if one wishes a bowl to "sing" in different modes – such behaviour is easier to obtain in larger bowls. As a concluding remark, we stress that a sonorous bowl/puja rattling contact can easily arise, in particular at higher tangential velocities and lower normal forces, a feature which was equally displayed by many experiments and numerical simulations, as discussed before.

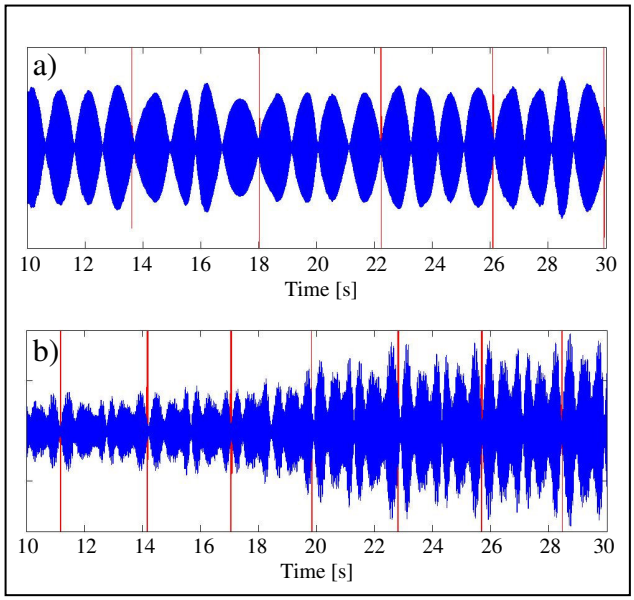


Figure 18 – Near-field sound pressure waveform (blue) due to friction excitation by: a) a rubber-covered *puja* and b) a wooden *puja* on Bowl 4, and electrical impulses (red) synchronized with the passage of the puja by the microphone position (sound files available).

## 6. Conclusions

In this paper we have developed a modelling technique based on the modal approach, which can achieve accurate

time-domain simulations of impacted and/or rubbed axi-symmetrical structures such as the Tibetan singing bowl.

To substantiate the numerical simulations, we performed an experimental modal analysis on three bowls. Results show the existence of 5 to 7 prominent vibrational mode-pairs up to frequencies about 6 kHz, with very low modal damping values. The numerical simulations presented in this paper show some light on the sound-producing mechanisms of Tibetan singing bowls. Both impact and friction excitations have been addressed, as well as perfectly-symmetrical and less-than-perfect bowls (a very common occurrence). For suitable friction parameters and for adequate ranges of the normal contact force $F_N$ and tangential rubbing velocity $V_T$ of the *puja*, instability of a shell mode (typically the first "elastic" mode, with 4 azimuthal nodes) arises, with an exponential increase of the vibration amplitude followed by saturation due to nonlinear effects.

Because of the intimate coupling between the radial and tangential shell motions, the effective bowl/*puja* contact force is not constant, but oscillates. After vibratory motions settle, the excitation point tends to locate near a nodal region of the *radial* motion of the unstable mode, which corresponds to an anti-nodal region of the friction-excited *tangential* motion (this effect is somewhat relaxed for softer *pujas*). This means that unstable modes spin at the same angular velocity of the *puja*. As a consequence, for the listener, sounds will always be perceived with beating phenomena. However, for a perfectly symmetrical bowl, no beating at all is generated at the moving excitation point.

Typically, the transient duration increases with $V_T$ and decreases for higher values of $F_N$. The way vibratory amplitudes depend on $V_T$ and $F_N$ changes for different response regimes. Three basic motion regimes were obtained in the present computations, depending on $F_N$ and $V_T$: (1) Steady self-excited vibration with permanent contact between the *puja* and the bowl; (2) Steady self-excited vibrations with periodic contact disruption; (3) Unsteady self-excited vibrations with intermittent amplitude increasing followed by attenuation after chaotic chattering.

It was demonstrated through computations and experiments that the order $j$ of the mode triggered by friction excitation is heavily dependent on the contact/friction parameters. In our computations and experiments on a large bowl, the first mode responded easily when using a soft high-friction *puja*, while instability of the second mode was triggered by using a harder lower-friction wooden *puja*.

The first motion regime offers the "purest" bowl singing. Our results suggest that higher values of $F_N$ should enable a better control of the produced sounds, as they lead to shorter transients and also render the system less prone to chattering.

As a concluding note, the computational methods presented in this paper can be easily adapted for the dynamical simulation of glass harmonicas, by simply changing the modes of the computed system, as well as the contact and friction parameters.

## Acknowledgments

This work has been endorsed by the Portuguese *Fundação para a Ciência e Tecnologia* under grant SFRH/BD/12806/2003.

## References

[1] A. Akay, "Acoustics of Friction", Journal of the Acoustical Society of America 111, pp. 1525-1547 (2002).

[2] T. D. Rossing, "The Science of Percussion Instruments", Singapore, World Scientific, (2000).

[3] A. P. French, "In Vino Veritas: A Study of Wineglass Acoustics", American Journal of Physics 51, pp. 688-694 (1983).

[4] T. D. Rossing, "Acoustics of the Glass Harmonica", J. Acoust. Soc. Am. 95, pp. 1106-1111 (1994).

[5] J.-C. Chapuis, "Ces Si Délicats Instruments de Verre", Pour la Science 272, pp. 68-74, (2000).

[6] G. Essl and P. Cook, "Measurement and Efficient Simulations of Bowed Bars", Journal of the Acoustical Society of America 108, pp. 379-388 (2000)

[7] O. Inácio, L. Henrique, J. Antunes, "Dynamical Analysis of Bowed Bars", Proceedings of the 8th

International Congress on Sound and Vibration (ICSV8), Hong Kong, China (2001).

[8] O. Inácio, L. Henrique, J. Antunes, "Simulation of the Oscillation Regimes of Bowed Bars: A Nonlinear Modal Approach", Communications in Nonlinear Science and Numerical Simulation, Vol. 8, pp. 77-95 (2003).

[9] O. Inácio, L. Henrique, J. Antunes, "Nonlinear Dynamics and Playability of Bowed Instruments: From the Bowed String to the Bowed Bar", Proceedings of the Eleventh International Conference on Computational Methods and Experimental Measurements (CMEM 2003), Halkidiki, Greece (2003).

[10] P. Cook, "Real Sound Synthesis for Interactive Applications", A. K. Peters, Natick, Massachusetts, USA (2002).

[11] S. Serafin, C. Wilkerson, J. Smith III, "Modelling Bowl Resonators Using Circular Waveguide Networks", Proceedings of the 5th International Conference on Digital Audio Effects (DAFx-02), Hamburg, Germany (2002).

[12] D. Young, G. Essl, "HyperPuja: A Tibetan Singing Bowl Controller", Proceedings of the Conference on New Interfaces for Musical Expression (NIME-03), Montreal, Canada (2003).

[13] O. Inácio, L. Henrique, J. Antunes, "The Physics of Tibetan Singing Bowls – Part 1: Theoretical Model and Part 2: Numerical Simulations", 34th National Acoustics Congress and Acoustics Iberian Meeting (TecniAcustica 2003), Bilbao, Spain (2003).

[14] O. Inácio, J. Antunes, "Dynamical Responses of a Large Tibetan Singing Bowl", Proceedings of the International Symposium on Musical Acoustics, (ISMA2004), Nara, Japan (2004).

[15] J. Antunes, M. Tafasca, L. Borsoi, "Simulation des Régimes Vibratoires Non-Linéaires d'Une Corde de Violon", Bulletin de la Société Française de Mécanique, Nº 2000-3, pp. 193-202 (2000).

[16] J. Antunes, L. Henrique, O. Inácio, "Aspects of Bowed-String Dynamics", Proceedings of the 17th International Congress on Acoustics, (ICA 2001), Roma, Italy (2001).

[17] O. Inácio, "Largeur d'Archet et Régimes Dynamiques de la Corde Frottée", Actes du 6e Congrès Français d'Acoustique (CFA 2002), Lille, France (2002).

[18] O. Inácio, J. Antunes, M.C.M. Wright, "On the Violin Family String/Body Dynamical Coupling", Proceedings of the Spring Conference of the Institute of Acoustics, Southampton, UK (2004).

[19] L. Henrique, J. Antunes, "Optimal Design and Physical Modelling of Mallet Percussion Instruments (Parts 1 and 2)", Actes du 6e Congrès Français d'Acoustique (CFA 2002), Lille, France (2002). Also in Acta Acustica (2003).

[20] M. L. Gaynor, "The Healing Power of Sound: Recovery from Life-threatening Illness Using Sound, Voice and Music", Shambhala Publications (2002).

[21] A. R. Thrasher, "Qing" in Stanley Sadie (ed.), The New Grove Dictionary of Music and Musicians, 2nd ed., New York, Macmillan, vol. 20, pp. 652 (2001).

[22] E. R. Jansen, "Singing Bowls: a Practical Handbook of Instruction and Use", Red Wheel (1993).

[23] A. Huyser, "Singing Bowl Exercises for Personal Harmony", Binkey Kok Publications, Havelte (1999).

[24] K. Gardner, "Sounding the Inner Landscape: Music as Medicine", Element, Rockport (1990).

[25] M. L. Gaynor, "Sounds of Healing: A Physician Reveals the Therapeutic Power of Sound, Voice, and Music", Bantam Dell Pub Group (1999).

[26] D. J. Ewins, "Modal Testing Theory and Practice", Wiley, New York, USA (1984).

[27] C. M. Harris, "Shock and Vibration Handbook", McGraw Hill, New York, 1996.

[28] J. T. Oden, J. A. C. Martins, "Models and Computational Methods for Dynamic Friction Phenomena", Computer Methods in Applied Mechanics and Engineering 52, 527-634 (1985).

[29] Beeman D., "Some Multistep Methods for Use in Molecular Dynamics Calculations", Journal of Computational Physics, Vol. 20, pp. 130-139 (1976).